PHYSICAL REVIEW B **89**, 161305(R) (2014)

Real-time electrical detection of coherent spin oscillations

Felix Hoehne,* Christian Huck, and Martin S. Brandt
Walter Schottky Institut, Technische Universität München, Am Coulombwall 4, 85748 Garching, Germany

Hans Huebl
Walther-Meißner-Institut, Bayerische Akademie der Wissenschaften, Walther-Meißner-Straße 8, 85748 Garching, Germany

(Received 29 July 2013; revised manuscript received 5 March 2014; published 21 April 2014)

We demonstrate that the bandwidth of pulsed electrically detected magnetic resonance can be increased to at least 80 MHz using a radio-frequency-reflectometry detection scheme. Using this technique, we measure coherent spin oscillations in real time during a resonant microwave pulse. We find that the observed signal is in quantitative agreement with simulations based on rate equations modeling the recombination dynamics of the spin system under study. The increased bandwidth opens the way to electrically study faster spin-dependent recombination processes, e.g., in direct semiconductors which so far have almost exclusively been studied by optically detected magnetic resonance.

DOI: 10.1103/PhysRevB.89.161305 PACS number(s): 75.76.+j, 71.55.Cn, 72.20.Jv, 76.30.−v

Recombination processes are ubiquitous in bipolar semiconductor devices such as inorganic or organic light-emitting diodes and solar cells. Particularly valuable information can be obtained when a recombination process is spin-dependent since this allows for the spectroscopic identification of the participating charge carriers, recombination centers, or charge transfer complexes via their spin signatures [1–5] by using methods such as optically or electrically detected magnetic resonance (ODMR and EDMR, respectively) [6,7]. In addition, by means of coherent spin manipulation and pulsed optical excitation of charge carriers, highly relevant information on charge carrier dynamics can be obtained, allowing one to determine, e.g., trapping and recombination times [8,9]. To this end, complex sequences consisting of microwave (mw) and radio-frequency (rf) pulses for electron and nuclear spin manipulation and light pulses for carrier excitation have been developed [10,11]. However, in the case of pulsed EDMR (pEDMR) the finite bandwidth of conventional preamplifier-based current measurement setups limits the time resolution to some microseconds. For the observation of phenomena faster than that like coherent spin oscillations or fast recombination processes one therefore resorts to an indirect detection technique which allows one to reconstruct the state of the different spin ensembles relevant for the recombination by measuring the spin-dependent part of the current transient after the pulse sequence [12]. If, e.g., the coherent driving of a particular spin ensemble in a Rabi oscillation experiment is to be monitored, this requires the measurement of a separate transient for each driving pulse length followed by a reconstruction of the Rabi oscillation from an analysis of these transients [13,14]. Moreover, this method is only applicable to spin systems where at least one of the spin-dependent time constants is sufficiently long to be detected with the available measurement bandwidth. For continuous wave (cw) EDMR, it has been demonstrated [15] that the detection bandwidth can be increased by more than one order of magnitude employing an rf-reflectometry-based detection scheme [16,17]. Here, we combine this detection scheme with pulsed spin manipulation and use it to observe coherent spin oscillations in real time during the mw pulse, in contrast to the reconstruction from the photocurrent transient after the pulse. Furthermore, with the help of a quantitative model we show that the signal intensity of real-time pulsed EDMR and its time dependence are in very good agreement with the results of the conventional pulsed EDMR.

In pulsed EDMR [12,13], most signals can be described in terms of weakly coupled spin pairs, where the recombination rate between two paramagnetic localized states depends on the relative orientation of the two spins [red and blue arrows in Fig. 1(a)] [18]. Spin pairs with an antiparallel orientation of the two spins recombine rapidly, while parallel spin pairs are stable on a much longer time scale. Therefore, under above-band-gap illumination a steady state develops with almost all spin pairs in the parallel state. Resonant excitation of one of the two spins by mw irradiation increases the number of antiparallel spin pairs and consequently also the recombination rate which results in a resonant decrease of the photoconductivity. In the most simple pulsed EDMR experiment illustrated in Fig. 1(a), a resonant mw pulse causes one of the two spins (blue arrow) to coherently oscillate between its eigenstates. This changes the symmetry of the spin pair resulting in an oscillation of the overall recombination rate. The frequency of this oscillation (tens of MHz) is chosen much faster than the typical decoherence rates [19] and, therefore, in many cases larger than the bandwidth of most EDMR current detection setups (usually below 1 MHz) preventing the direct observation of these oscillations and requiring a reconstruction from an analysis of the current transient after the pulse [12]. In the following, we demonstrate that the limitations of this indirect detection scheme can be overcome by rf reflectometry allowing one to detect the coherent spin oscillations during the mw pulse.

The samples used in this work were grown by chemical vapor deposition and consist of a nominally 22-nm-thick Si layer with a P concentration of $\sim 3 \times 10^{16}$ cm^{-3} on a 2.5-μm-thick, undoped Si buffer grown on a (100)-oriented silicon-on-insulator substrate. The doped epilayer leads to a dominant ^{31}P-P_{b0} recombination [20], where the P_{b0} spin

*hoehne@wsi.tum.de

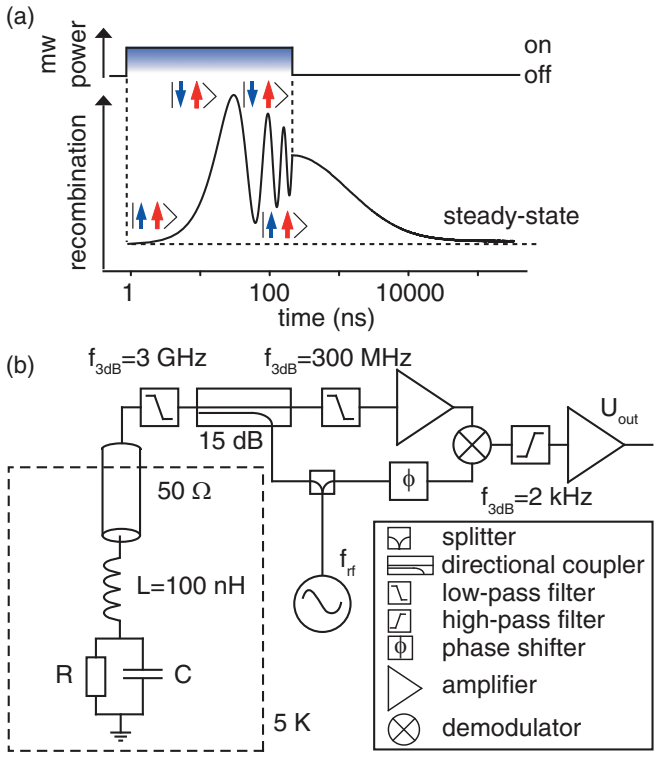

FIG. 1. (Color online) (a) Basic concept of a pulsed EDMR measurement. The symmetry of the spin pair determines the recombination rate with parallel spin pairs recombining much slower than antiparallel spin pairs due to the Pauli principle. While conventional pulsed EDMR can only assess the state of the spin pair at the end of the mw pulse by measuring the photocurrent transient, rf-EDMR can directly monitor the coherent spin oscillations during the mw pulse shown on a logarithmic time scale. (b) Schematic of the rf-EDMR LCR tank circuit and homodyne detection setup.

partners are defect states at the interface of the doped epilayer and the natural oxide formed on top [21]. All experiments are performed at 5 K under illumination with red light of a light-emitting diode (LED) (photon energy $h\nu = 1.95$ eV) in a dielectric mw resonator for pulsed EPR at X-band frequencies. Interdigit Cr/Au electrical contacts with a periodicity of 10 μm are evaporated on an area of 2×2 mm^2.

For rf reflectometry, a chip inductance of $L = 100$ nH is placed between the sample and a 50 Ω coplanar waveguide (CPW), which connects the sample to the room-temperature electronics via a 50 Ω coaxial cable [Fig. 2(b)]. The sample resistance R, its stray capacitance C, and the inductance L form a resonant LCR tank circuit with a resonance frequency of $f_0 \approx 1/\sqrt{LC}$ whose impedance can be matched to 50 Ω by varying R via the illumination intensity. Measuring the reflected rf power as a function of the radio frequency $f_{\rm rf}$ using a vector network analyzer, we find a resonance frequency of $f_0 = 190$ MHz and a bandwidth (FWHM) of $\sim$80 MHz [Fig. 2(a)]. For rf-EDMR measurements, we use the rf-reflectometry homodyne detection setup shown in Fig. 1(b). It is calibrated for resistance measurements by simultaneously measuring the output voltage of the demodulator $U_{\rm out}$ at $f_{\rm rf} = f_0 = 190$ MHz and the dc sample resistance R as a function of the illumination intensity. From this, we obtain a relation

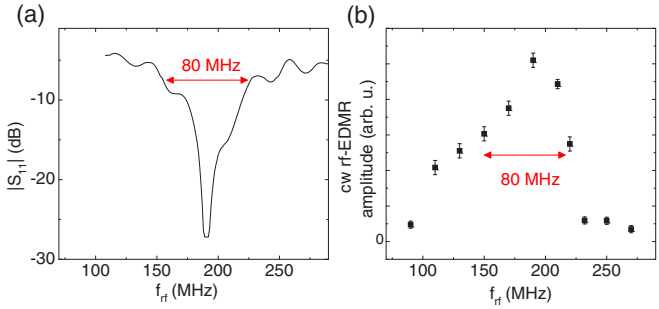

FIG. 2. (Color online) (a) Absolute value of the reflection coefficient $|S_{11}|$ as a function of the rf $f_{\rm rf}$. (b) Amplitude of the high-field ^{31}P hyperfine peak measured by cw rf-EDMR as a function of $f_{\rm rf}$.

between $U_{\rm out}$ and R revealing a linear dependence around the working point. The shape of the resonant dip [Fig. 2(a)] deviates from the expected Lorentzian shape most likely due to spurious reflections at the transitions between the coaxial cable and the CPW and between the CPW and the sample. From the resonance frequency and the value of the inductance, we calculate a capacitance of $C = 1/L(2\pi f_0)^2 = 7$ pF in good agreement with the estimated capacitance of the interdigit contact structure of $\sim$14 pF [22].

In a next step, we use this measurement scheme to detect the change of R induced by the resonant excitation of ^{31}P spin transitions in cw rf-EDMR. For this purpose, the sample is continuously irradiated with microwaves with the frequency of 9.739 GHz chosen such that the spectrally isolated high-field ^{31}P hyperfine-split electron spin transitions are resonantly excited at a magnetic field of $B_0 = 350.6$ mT [blue arrow in the spectrum in Fig. 3(b)]. The amplitude of the ^{31}P signal shown in Fig. 2(b) as a function of $f_{\rm rf}$ is maximal for $f_{\rm rf} = f_0 = 190$ MHz and decreases to almost zero for $f_{\rm rf} > 250$ MHz or $f_{\rm rf} < 100$ MHz. These results directly reflect the frequency-dependent sensitivity of the rf-reflectometry setup which is maximal when $f_{\rm rf}$ matches the resonance frequency of the LCR resonator and close to zero for $f_{\rm rf}$ far away from the resonance [16,17]. The frequency range over which an EDMR signal is observed [red arrow in Fig. 2(b)] agrees well with the bandwidth of 80 MHz determined in Fig. 2(a) confirming that the rf reflectometry indeed should allow EDMR measurements with a time resolution of tens of nanoseconds.

In the following, we use the large detection bandwidth of rf-EDMR to observe coherent spin oscillations during the mw excitation pulse as summarized in Fig. 3. To this end, we irradiate the sample with a 2-μs-long mw pulse at the fixed frequency of 9.739 GHz and simultaneously measure the time dependence of R during and after the mw pulse. The results in Fig. 3(a) show the relative change of the sample resistance for three different values of B_0. Two of these values are chosen such that the mw pulse resonantly excites the ^{31}P and P_{b0} transitions (blue and red trace), while the third value is chosen off-resonant for comparison (black trace). The corresponding spectral positions are indicated by the according color-coded arrows in the pulsed rf-EDMR spectrum shown in Fig. 3(b). The resistance first increases during the mw pulse and decreases after the pulse with a time constant of ~ 5 μs for the two resonant transients, while no variation is observed

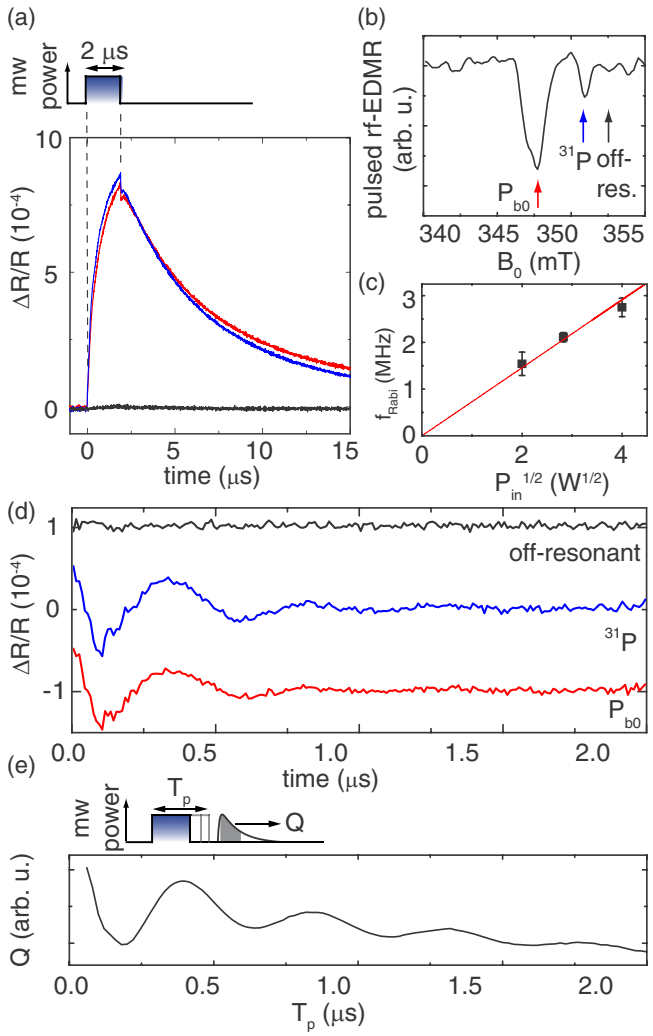

FIG. 3. (Color online) (a) Relative change of the sample resistance for different magnetic fields chosen such that the mw pulse resonantly excites the ^{31}P spins (blue), the P_{b0} spins (red), or none of the spins (black). To improve the signal-to-noise ratio, a lock-in detection scheme [23] is implemented employing square-wave frequency modulation with a frequency of 500 Hz. (b) Pulsed rf-EDMR spectrum recorded by boxcar integration of the $\Delta R/R$ transient after a 9.739 GHz mw pulse as a function of the magnetic field B_0. The spectral positions of the mw pulses used in (a) are indicated by the color-coded arrows. (c) Frequency of the oscillations f_{Rabi} depicted in (d) as a function of the square root of the mw power P_{in} showing a linear dependence (red line). (d) First two microseconds of the transients from (a) after subtraction of a second order polynomial background revealing oscillations on the two resonant traces. (e) Coherent spin oscillations measured by reconstructing the spin state after mw pulses of varying length T_{p} [13]. To this end, the preamplifier-detected current transient after each pulse is integrated resulting in a charge Q proportional to the number of antiparallel spin pairs at the end of the pulse.

in the off-resonant transient [Fig. 3(a)]. We attribute the fast initial drop after the mw pulse to an imperfect subtraction of the nonresonant background. The maximum value of $\Delta R/R \approx 7 \times 10^{-4}$ is comparable to the maximum change of $\Delta R/R \approx 10^{-3}$ observed in conventionally detected pulsed EDMR experiments on this sample. During the mw pulse, a weak oscillation with a period of 500 ns is present on the two resonant traces, which is revealed after subtraction of a second order polynomial background as shown in Fig. 3(d), while it is not observed for the off-resonant trace. We attribute these oscillations to the changes in the recombination rate caused by coherent spin oscillations during the mw pulse observed in real time [Fig. 1(a)]. For comparison, coherent oscillations measured by conventionally detected pulsed EDMR [13] are shown in Fig. 3(e), exhibiting the same oscillation frequency as those measured by rf reflectometry. Our interpretation is further confirmed by the linear dependence of the oscillation frequency f_{Rabi} of the pulsed rf-EDMR on the square root of the mw power [Fig. 3(c)]. For higher mw powers, the noise level caused by the strong mw pulses increases while the oscillation amplitude decreases, as discussed below, impeding the observation of faster oscillations in these samples.

The oscillation amplitude of $\sim 5 \times 10^{-5}$ is much smaller than the overall resonant resistance change of $\sim 7 \times 10^{-4}$. The small amplitude of the oscillation results from two conflicting conditions which have to be met in order to observe the recombination process. On the one hand, the recombination has to be sufficiently fast compared to the oscillation period of the spin, so that the change of the spin pair state is reflected instantaneously in the photocurrent. On the other hand, however, the spin pairs are destroyed by the recombination process leading to a rapid decay of the oscillation for recombination processes much faster than the oscillation period.

To gain quantitative insight into this, we calculate the change of the photoconductivity by modeling the dynamics of the spin pair based on a set of rate equations extending the approach of Ref. [9] by explicitly including the spin dynamics during the mw pulse. In the following discussion, we use three states, namely, the parallel state of the spin pair $|1\rangle$, the antiparallel state $|2\rangle$, and the ionized $^{31}\mathrm{P}^{+}$-P_{b0}^{-} state $|3\rangle$ as sketched in Fig. 4(a). The time evolution of the corresponding

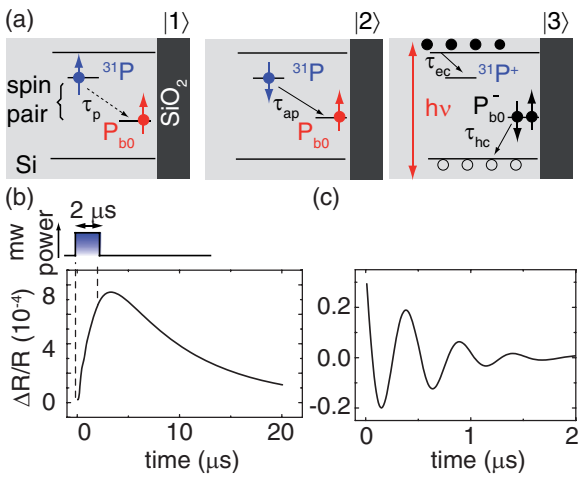

FIG. 4. (Color online) (a) Definition of the time constants of the ^{31}P-P_{b0} recombination process. (b) Simulation of the relative resistance change during and after a 2 -μs-long mw pulse. (c) First 2 μs of the data shown in panel (a) after subtraction of a second order polynomial background.

density matrix $\rho(t)$ is calculated by a master equation

$$\frac{d\rho}{dt} = \frac{i}{\hbar}[\hat{H},\rho] + \tilde{R}\cdot\rho. \tag{1}$$

The first part of Eq. (1) describes the coherent evolution during the mw pulse, while the second part describes the recombination process.

To simplify the discussion, we further neglect the coherences between states $|1\rangle$ and $|3\rangle$ and between $|2\rangle$ and $|3\rangle$, since the recombination process is incoherent. Writing the remaining terms of ρ as a column vector $\tilde{\rho} = (\rho_{11},\rho_{12},\rho_{21},\rho_{22},\rho_{33})^{\mathrm{T}}$, the recombination operator $\tilde{R}$ becomes

$$\tilde{R} = \begin{pmatrix} -\frac{1}{\tau_p} & 0 & 0 & 0 & \frac{1}{2\tau_g} \\ 0 & -\frac{\tau_p+\tau_{ap}}{2\tau_p\tau_{ap}} - \frac{1}{T_d} & 0 & 0 & 0 \\ 0 & 0 & -\frac{\tau_p+\tau_{ap}}{2\tau_p\tau_{ap}} - \frac{1}{T_d} & 0 & 0 \\ 0 & 0 & 0 & -\frac{1}{\tau_{ap}} & \frac{1}{2\tau_g} \\ \frac{1}{\tau_p} & 0 & 0 & \frac{1}{\tau_{ap}} & -\frac{1}{\tau_g} \end{pmatrix}, \tag{2}$$

with the recombination time of parallel spin pairs τ_p, the recombination time of antiparallel spin pairs τ_{ap}, and formation time constants of new spin pairs τ_g with $1/\tau_g = 1/\tau_{ec} + 1/\tau_{hc}$, where τ_{ec} and τ_{hc} denote the time constants of an electron and hole capture process, respectively, as defined in Fig. 4(a) and Refs. [9,11]. We additionally included the dephasing time T_d to account for the experimentally observed dephasing of the coherent spin oscillations [Figs. 3(d) and 3(e)], which we attribute to inhomogeneities in the driving mw magnetic field.

The operator $\tilde{H}\cdot\tilde{\rho} = \frac{i}{\hbar}[\hat{H},\rho]$ describing the coherent evolution of $\tilde{\rho}$ in the rotating frame during a mw pulse, which selectively excites one of the two weakly coupled spins, then takes the form

$$\tilde{H} = i\frac{\omega_{\mathrm{Rabi}}}{2}\begin{pmatrix} 0 & 1 & -1 & 0 & 0 \\ -1 & 0 & 0 & 1 & 0 \\ 1 & 0 & 0 & -1 & 0 \\ 0 & -1 & 1 & 0 & 0 \\ 0 & 0 & 0 & 0 & 0 \end{pmatrix}, \tag{3}$$

with the angular Rabi frequency ω_{Rabi}. In Eq. (3), we have taken into account that state $|3\rangle$ is not paramagnetic and therefore unaffected by the mw pulse. We numerically solve Eq. (1) by calculating

$$\tilde{\rho}(t) = \begin{cases} e^{(\tilde{H}+\tilde{R})t}\,\tilde{\rho}(0) & \text{during the mw pulse} \\ e^{\tilde{R}t}\,\tilde{\rho}(0) & \text{after the mw pulse,} \end{cases} \tag{4}$$

with $\tilde{\rho}(0) = (1,0,0,0,0)^{\mathrm{T}}$ assuming that the spin system is in the parallel state at the beginning of the mw pulse.

Finally, we calculate the relative change of the resistance $\Delta R(t)/R = c\cdot\Delta\tilde{\rho}_{33}(t)$ [9], with $\Delta\tilde{\rho}_{33}(t) = \tilde{\rho}_{33}(t) - \tilde{\rho}_{33}(0)$ and a proportionality constant c. The resulting $\Delta R(t)/R$ is plotted in Fig. 4(a), using the fixed parameters $\tau_p = 1200\ \mu$s and $\tau_{ap} = 2\ \mu$s [9], while $\tau_g = 2.6\ \mu$s, $T_d = 210$ ns, and $c = 2.3\times10^{-3}$ are used as fitting parameters to match the experimental data in Fig. 3(a).

The simulated transient reproduces the basic features of the experimental data in Fig. 3(a) with characteristic rise and fall times determined mainly by τ_{ap} and τ_g, respectively. Again, the coherent oscillations during the mw pulse are revealed after subtraction of a second order polynomial background as shown in Fig. 4(c). The oscillation amplitude of $\sim2\times10^{-5}$ is a factor of $\sim$40 smaller compared to the simulated maximum total change of the resistance in good agreement with the experimentally observed suppression by a factor of $\sim$20. We therefore conclude that the time constants of the recombination process naturally explain the observed shape of the transient as well as the amplitude of the coherent oscillations. The experimentally observed decay of the transient after the mw pulse has a stretched exponential character [Fig. 3(a)], which we attribute to a distribution of recombination and generation time constants over the spin pair ensemble [9] not taken into account by the simulation. We note that the observed signal-to-noise ratio of the pulsed rf-EDMR [Fig. 3(d)] is by a factor of 40–80 lower compared to the conventionally recorded spectrum [Fig. 3(e)]. In addition to the recombination rate induced factor of 20, we expect an additional decrease of the signal-to-noise ratio by a factor of 9 due to the increase of the bandwidth from 1 to 80 MHz.

In conclusion, we implemented rf-reflectometry readout for pulsed EDMR thereby increasing the measurement bandwidth by almost two orders of magnitude compared to current preamplifier-based detection schemes. This opens the way to studying faster charge dynamics, e.g., in direct semiconductors which with very few exceptions [3,24–26] so far have almost exclusively been studied by ODMR because of their shorter carrier lifetimes compared to indirect semiconductors such as silicon. In direct semiconductors, rf-EDMR complements ODMR since it allows one to detect nonradiative recombination processes. Other systems that might benefit from the increased bandwidth are formation and dissociation processes of spin pairs in organic semiconductors [27,28], donor-bound excitons in silicon [29,30], and systems with short decoherence or relaxation times such as, e.g., GaAs [31]. When applying rf reflectometry to device structures such as diodes [3,24] or two-dimensional electron gases [14,32,33], where no illumination is needed for EDMR measurements, a significant reduction of the noise level is expected [15]. In particular, when spin-dependent scattering processes are detected, the large sensitivity of EDMR and the high time resolution demonstrated here might enable the observation and feedback control of spin fluctuations in small spin ensembles [34,35]. The presented rf-pEDMR technique can also be extended to higher tank circuit frequencies in the GHz range using contactless detection schemes [36].

This work was financially supported by DFG (Grant No. SFB 631, C3).

[1] H. Dersch, L. Schweitzer, and J. Stuke, Phys. Rev. B **28**, 4678 (1983).

[2] W. M. Chen, B. Monemar, E. Janzen, and J. L. Lindström, Phys. Rev. Lett. **67**, 1914 (1991).

[3] W. E. Carlos, E. R. Glaser, T. A. Kennedy, and S. Nakamura, Appl. Phys. Lett. **67**, 2376 (1995).
[4] V. Dyakonov, G. Rösler, M. Schwoerer, S. Blumstengel, and K. Lüders, J. Appl. Phys. **79**, 1556 (1996).
[5] M. Stutzmann, M. S. Brandt, and M. W. Bayerl, J. Non-Cryst. Solids **266-269**, 1 (2000).
[6] N. C. Greenham, J. Shinar, J. Partee, P. A. Lane, O. Amir, F. Lu, and R. H. Friend, Phys. Rev. B **53**, 13528 (1996).
[7] J.-M. Spaeth and H. Overhof, *Point Defects in Semiconductors and Insulators* (Springer, Berlin, 2003).
[8] G. W. Morley, D. R. McCamey, H. A. Seipel, L.-C. Brunel, J. van Tol, and C. Boehme, Phys. Rev. Lett. **101**, 207602 (2008).
[9] F. Hoehne, L. Dreher, M. Suckert, D. P. Franke, M. Stutzmann, and M. S. Brandt, Phys. Rev. B **88**, 155301 (2013).
[10] L. Childress, M. V. Gurudev Dutt, J. M. Taylor, A. S. Zibrov, F. Jelezko, J. Wrachtrup, P. R. Hemmer, and M. D. Lukin, Science **314**, 281 (2006).
[11] L. Dreher, F. Hoehne, M. Stutzmann, and M. S. Brandt, Phys. Rev. Lett. **108**, 027602 (2012).
[12] C. Boehme and K. Lips, Phys. Rev. B **68**, 245105 (2003).
[13] A. R. Stegner, C. Boehme, H. Huebl, M. Stutzmann, K. Lips, and M. S. Brandt, Nat. Phys. **2**, 835 (2006).
[14] T. Machida, T. Yamazaki, K. Ikushima, and S. Komiyama, Appl. Phys. Lett. **82**, 409 (2003).
[15] H. Huebl, R. P. Starrett, D. R. McCamey, A. J. Ferguson, and L. H. W. van Beveren, Rev. Sci. Instrum. **80**, 114705 (2009).
[16] R. J. Schoelkopf, P. Wahlgren, A. A. Kozhevnikov, P. Delsing, and D. E. Prober, Science **280**, 1238 (1998).
[17] S. J. Angus, A. J. Ferguson, A. S. Dzurak, and R. G. Clark, Appl. Phys. Lett. **92**, 112103 (2008).
[18] D. Kaplan, I. Solomon, and N. F. Mott, J. Phys. Lett. (Paris) **39**, 51 (1978).
[19] H. Huebl, F. Hoehne, B. Grolik, A. R. Stegner, M. Stutzmann, and M. S. Brandt, Phys. Rev. Lett. **100**, 177602 (2008).
[20] F. Hoehne, H. Huebl, B. Galler, M. Stutzmann, and M. S. Brandt, Phys. Rev. Lett. **104**, 046402 (2010).
[21] A. Stesmans and V. V. Afanas'ev, J. Appl. Phys. **83**, 2449 (1998).
[22] H.-E. Endres and S. Drost, Sens. Act. B: Chem. **4**, 95 (1991).
[23] F. Hoehne, L. Dreher, J. Behrends, M. Fehr, H. Huebl, K. Lips, A. Schnegg, M. Suckert, M. Stutzmann, and M. S. Brandt, Rev. Sci. Instrum. **83**, 043907 (2012).
[24] M. W. Bayerl, M. S. Brandt, and M. Stutzmann, Phys. Status Solidi A **159**, R5 (1997).
[25] T. Wimbauer, M. S. Brandt, M. W. Bayerl, N. M. Reinacher, M. Stutzmann, D. M. Hofmann, Y. Mochizuki, and M. Mizuta, Phys. Rev. B **58**, 4892 (1998).
[26] D. Stein, K. v. Klitzing, and G. Weimann, Phys. Rev. Lett. **51**, 130 (1983).
[27] F. Grozema, L. Siebbeles, J. Warman, S. Seki, S. Tagawa, and U. Scherf, Adv. Mater. **14**, 228 (2002).
[28] T. Virgili, G. Cerullo, L. Lüer, G. Lanzani, C. Gadermaier, and D. D. C. Bradley, Phys. Rev. Lett. **90**, 247402 (2003).
[29] W. Schmid, Phys. Status Solidi B **84**, 529 (1977).
[30] M. Steger, K. Saeedi, M. L. W. Thewalt, J. J. L. Morton, H. Riemann, N. V. Abrosimov, P. Becker, and H.-J. Pohl, Science **336**, 1280 (2012).
[31] R. Hanson, L. P. Kouwenhoven, J. R. Petta, S. Tarucha, and L. M. K. Vandersypen, Rev. Mod. Phys. **79**, 1217 (2007).
[32] C. F. O. Graeff, M. S. Brandt, M. Stutzmann, M. Holzmann, G. Abstreiter, and F. Schäffler, Phys. Rev. B **59**, 13242 (1999).
[33] C. C. Lo, V. Lang, R. E. George, J. J. L. Morton, A. M. Tyryshkin, S. A. Lyon, J. Bokor, and T. Schenkel, Phys. Rev. Lett. **106**, 207601 (2011).
[34] R. Budakian, H. J. Mamin, B. W. Chui, and D. Rugar, Science **307**, 408 (2005).
[35] S. T. B. Goennenwein, M. W. Bayerl, M. S. Brandt, and M. Stutzmann, Phys. Rev. Lett. **84**, 5188 (2000).
[36] L. S. Vlasenko, Y. V. Martynov, T. Gregorkiewicz, and C. A. J. Ammerlaan, Phys. Rev. B **52**, 1144 (1995).